Blood Pressure Monitoring with Difference of Gaussians and Deep Learning

Sung Woo Kim[1], Jae Young Lee[2], and Junmo Kim[2]

[1] ZTACOM, Seoul, South Korea
ksw@ztacom.com
[2] KAIST, Daejeon, South Korea
{mcneato,junmo.kim}@kaist.ac.kr

Abstract. We introduce an arterial blood pressure reconstruction method from photoplethysmography signals obtained by a cuff-less device. The proposed method is built upon a UNet-based architecture with the difference of Gaussian (DoG) attention module. With multi-scale features from the encoder of the UNet, the DoG attention block emphasizes important sub-band frequency parts of features, ultimately leading to improved blood pressure estimation performance. Utilizing the MIMIC-III dataset, which comprises over 12,000 records, the proposed method shows better performance than the existing methods in the Association for British Hypertension Society standard and reasonable performance in the Advancement of Medical Instrumentation standard. In the future, we hope that deploying the proposed method in a sensor robot or a wearable device can lead to widespread use in personal health management and remote patient monitoring scenarios.

Keywords: arterial blood pressure, ABP, photoplethysmography, PPG, wearable device, signal reconstruction, sensing robot.

1 Introduction

Recently, the lifestyle and dietary habits of modern people are contributing to an increasing risk of cardiovascular diseases. Factors such as the rise in processed foods, high intake of salt and fat, lack of exercise, and a stress-ridden environment are elevating the risk factors for cardiovascular diseases. These factors impose a continuous burden on the heart and blood vessels, leading to unstable blood pressure and causing major health issues [13]. Therefore, managing blood pressure (BP) is not optional for modern people; it is essential.

There are various methods to monitor BP. In the past, a catheter had been inserted into an artery for invasive measurement. However, it can lead to various adverse effects, such as pain, infection, and arterial damage due to the insertion of the catheter. Recently, to avoid adverse effects, BP has been measured non-invasively using a cuff-based sphygmomanometer, even in the intensive care units (ICU). However, the non-invasive method of measuring BP also has its limitations [11]. First, the size of the measuring device restricts the places where it can be used. Second, it measures BP

only at the moment of measurement, which imposes restrictions on BP monitoring. Addressing these limitations and improving user convenience, several studies [2,7,8] have suggested monitoring BP by acquiring biometric data through wearable devices or sensing robots. This approach utilizes pulse transit time, pulse arrival time, and pulse wave analysis of the PPG and ECG signals to estimate BP. However, since PPG signals are highly susceptible to external noise [9], which frequently compromises the waveform, this method, which relies on hand-crafted calculated values, is only feasible in scenarios with ideal signal conditions. Thus, using deep learning, the reconstruction of the arterial blood pressure (ABP) waveform from PPG and ECG signals has been widely studied [9]. The ABP waveform contains information about systolic blood pressure (SBP), diastolic blood pressure (DBP), and mean arterial pressure (MAP), providing not only data on BP but also insights into cardiac output and blood pressure variability. Therefore, ABP waveform reconstruction enables monitoring not only BP estimates but also crucial physiological information related to the heart.

In this paper, we propose a PPG to ABP reconstruction method with the difference of Gaussians (DoG) attention and deep learning techniques. Specifically, we integrate the DoG attention block into a U-Net model. DoG attention block emphasizes transitions and edges, which are crucial for detailed feature extraction in signal processing. Therefore, when applied to PPG signals, which are sensitive to physiological and environmental noise, including movement, external light, and variations in skin thickness, the DoG attention block can emphasize the important part of signals. The DoG attention block is integrated within the skip connections of the U-Net model. Experimental results on the MIMIC-III dataset show that the proposed method outperforms the existing methods. In the future, by deploying the proposed method in sensing robots and wearable devices, we hope for continuous and unrestricted biometric monitoring.

2 Related Work

2.1 Arterial Blood Pressure Estimation

Based on deep learning techniques, various BP estimation methods [2,3,6,8,9,12,14] have been widely studied using the PPG signal. Although the previous BP estimation methods generally used a single PPG signal as an input, some methods utilized additional signals such as the velocity of PPG (VPG), acceleration of PPG (APG), or ECG to obtain more precise and detailed monitoring for their network input. The previous BP estimation methods are summarized according to their input types.

Method using a single PPG input: Various BP estimation methods [1,6,8,12,14] have utilized a single PPG signal for their input. Although various methods are built on the U-Net architecture [1,6,8,14], there are also methods based on other models such as the autoencoder [12] and handcrafted feature [15]. Athaya and Choi's method [1] predicts the delay between the PPG and ABP waveform, shifts the two signals accordingly, and reconstructs the ABP waveform. BP-Net [14] utilized various modified input PPG signals to enhance the signal-to-noise ratio in their network internally. PPG2ABP [6] generated the initial ABP waveform from the input PPG and utilized the initial ABP waveform as an independent variable. Then, using the ground truth ABP waveform as the dependent variable, the initial ABP waveform is refined to reconstruct the final ABP

waveform. SE-MSResUNet [8] integrated residual connections such as the inception and squeeze-and-excitation modules into a multiscale residual U-Net to reconstruct the ABP waveform. RDAE [12] utilized a deep autoencoder to learn compact and low-dimensional representations. Hybrid [15] proposed reconstructing the ABP waveform by combining an electrical network model, which represents the interconversion of flow and pressure in blood vessels, with a tube-load model that illustrates the propagation and reflection of pressure waves within the vascular structure.

Method using multiple inputs: Using PPG, VPG, and APG signals as their input, ABP-Net [3] utilized the blind source separation method designed for speech signals based on the U-Net. Using PPG, VPG, APG, and ECG signals as input, NABNet [9] proposed a method that combines a SBP & DBP prediction model using machine learning and a UNet-based ABP estimation model with the attention gate.

The previous methods using multiple inputs generally show better performance than those using a single PPG input. Although we utilize only a single PPG signal as an input for our model, the proposed method generally performs better than the previous methods using multiple inputs.

2.2 Difference of Gaussian

In deep learning, DoG has been widely studied within various applications of image processing and computer vision. The applications have extended from traditional image enhancement to complex tasks in medical imaging and video surveillance, demonstrating a broad utility in emphasizing scale and spatial differences.

Fu *et al*. [5] utilized multi-scale DoG to assess the quality of screen content images. They used multi-scale DoG to capture and emphasize various image features across multiple scales. Yang *et al*. [16] used calibrated convolution with DoG attention to improve classification accuracy on visual datasets. In their method, DoG improves feature transformation in CNN by focusing on scale-invariant information. Zhang *et al*. [18] used the DoG mechanism, particularly for background subtraction in motion images. Using the DoG, their method not only suppresses background noise effectively but also preserves essential edge details, showing robustness in real-world applications. SBA-Net [4] utilized the DoG attention block in sub-band configurations to enhance the performance of polyp detection. SBA-Net showed the applicability of the DoG method in high-stakes medical contexts, underlying their value in critical healthcare diagnostics. Yazdi *et al*.'s [17] involves dividing a kernel into two rotating 'L'-shaped sections and computing the DoG between two sections as they rotate. In their method, the DoG improves edge detection performance, to adaptively respond to varying orientations and shapes within the image.

Similar to how DoG has been utilized in other applications, we use DoG attention in place of the simple skip connections in U-Net to emphasize the detail of the signals and features, ultimately improving the performance of reconstructed ABP signals in PPG to ABP reconstruction.

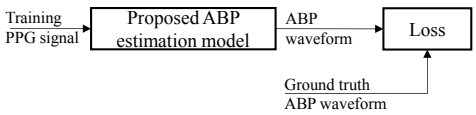

(a) ABP estimation train pipeline.

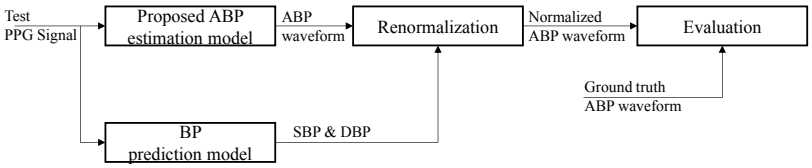

(b) ABP estimation test pipeline.

Fig. 1: The proposed ABP estimation method pipeline.

3 Method

3.1 Overall Pipeline

In Fig. 1, an overview of the proposed method for reconstructing the ABP waveform from the PPG signal using a deep-learning approach is presented. Fig. 1a shows the training pipeline for reconstructing the ABP waveform. For reconstructing the ABP waveform using the PPG signal, it is essential to address the inherent differences in the scale of signal amplitude between ABP & PPG signals and the variability that may exist among PPG signals. The ABP waveform, which includes critical BP information such as SBP and DBP, generally has a higher amplitude than the PPG signal. Consequently, to ensure a uniform influence of features on the model and to enhance generalization performance, the training process involves normalizing both the input PPG signal and the target ground truth ABP waveform to a range between 0 and 1. Our model utilizes the mean squared error (MSE) loss function during the training pipeline and uses the ground truth ABP waveforms.

Fig. 1b shows the integration of our proposed trained ABP waveform reconstruction model with the BP prediction model proposed in ShallowNet [10] to reconstruct the final ABP waveform, for testing. In the test phase, the reconstructed ABP waveform initially loses the amplitude information for SBP and DBP due to influential amplitude differences between the PPG signal and the ABP waveform. To address this, we utilize the estimated SBP and DBP values provided by ShallowNet [10] to restore the original amplitude information for SBP and DBP through a renormalization process. This approach enables the reconstructed ABP waveform to regain its original amplitude characteristics. The figure illustrates the evaluation process, which compares the reconstructed ABP waveform with the ground truth ABP.

3.2 Proposed Arterial Blood Pressure Estimation Method

The proposed method for reconstructing the ABP waveform leverages a deep learning architecture based on the U-Net, as shown in Fig. 2. The initial PPG signal input is

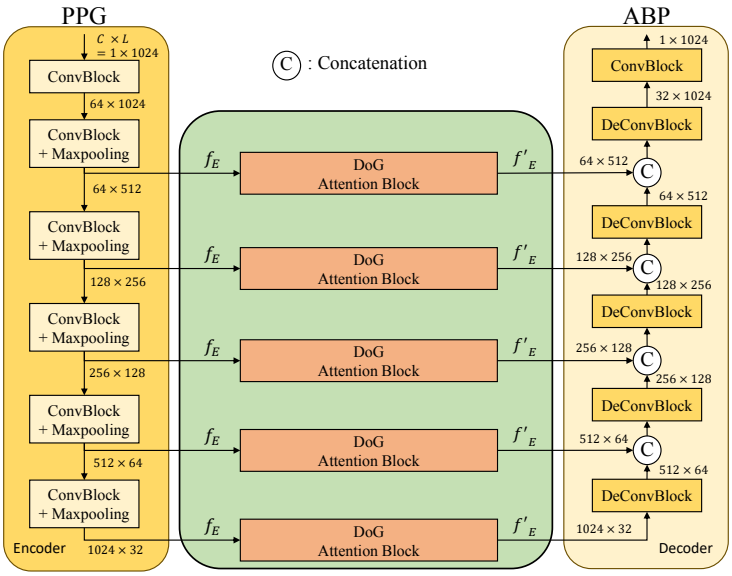

Fig. 2: The proposed ABP estimation architecture.

shaped into $C \times L = 1 \times 1024$ where C and L signify channel and signal length, respectively. The encoder consists of a series of convolutional blocks, each followed by max pooling. This process reduces the input signal's length by half and doubles the input channel while increasing the depth. After each convolution block, the output is directed in two distinct pathways where one stream flows through skip connections to the to enhance the feature maps with focused attention, and another stream continues deeper into the network's layers. The model then concatenates the output with the output from the corresponding deconvolutional block at the corresponding layer depth. This concatenation combines the enhanced feature maps from the DoG block, which are specifically optimized to emphasize crucial signal characteristics, with the broader spatial features from the deconvolutional block.

This process enriches the feature set available for reconstruction, enabling a more accurate rebuilding of the ABP waveform. As the signal through these progresses, it undergoes further deconvolutional processing, which expands the reduced dimensions back toward their original size. Ultimately, each deconvolutional stage incrementally increases the resolution of the feature maps while merging them with higher-resolution details from earlier in the network, preserved through the DoG attention block. This deconvolutional upscaling continues until the output dimensions are upscaled to the initial input size of 1×1024.

3.3 DoG attention mechanism

Fig. 3 which incorporates the DoG to enhance the ability to focus on significant features within the PPG signal. With the given signal f, The DoG filter $D(\cdot)$ in the DoG attention

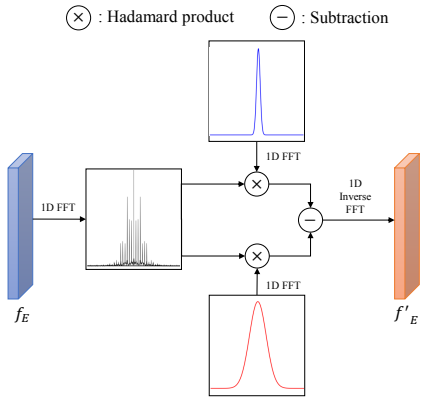

Fig. 3: The DoG attention block.

block is mathematically defined as

$$D(f) = G(f;\sigma_1) - G(f;\sigma_2), \tag{1}$$

where $G(f;\sigma)$ represents Gaussian function with the blurriness control variable σ. The variables σ_1 and σ_2 denote the distinct standard deviations for the two Gaussian filters, with σ_1 being less than σ_2 to accentuate finer details by emphasizing higher frequencies in $G(f;\sigma_1)$. This configuration is essential for highlighting the details in a signal by filtering frequencies selectively. Fig. 3 shows the flow of the DoG attention block. The DoG attention block leverages rich features f_E from the encoder to perform focused attention processing. The features are processed in the frequency domain. The input feature f_E is filtered using two different Gaussian kernels and the filtered features are subtracted. Finally, the subtracted feature f'_E is fed to the decoder. In the feature maps applying the DoG method, the DoG attention block highlights key features and suppresses irrelevant noise by contrasting Gaussian-blurred versions of the input feature maps at different scales. This selective attention helps emphasize significant physiological signals within the PPG data. The outputs from the DoG attention block are then concatenated with the feature maps from the outputs of the deconvolutional block. This concatenation of information enhances the model's ability to reconstruct the ABP waveform with high fidelity, ensuring that both detailed nuances and broader patterns are captured effectively. This mechanism enables our proposed method to facilitate a robust feature extraction and enhancement process that underpins the model's performance in ABP estimation.

4 Experiments

4.1 Dataset

We utilized the MIMIC-III waveform dataset available from the UCI database. The MIMIC-III includes 12,000 records of PPG, ECG signal, and ABP waveform data collected from the ICU. The data was preprocessed into four parts, each part containing

Table 1: Criteria for grading according to the BHS standard.

	BHS metric		
Grade	$\leq$ 5mmHg	$\leq$ 10mmHg	$\leq$ 15mmHg
A	60%	85%	95%
B	50%	75%	90%
C	40%	65%	85%
D	worse than C		

Table 2: Criteria for grading according to the AAMI standard.

	ME (mmHg)	SD (mmHg)	Number of Subjects
AAMI standard	$\leq$ 5mmHg	$\leq$ 8mmHg	$\geq$ 85

3,000 records. Each segment in every part of the dataset has 1,024 sample points with a frequency of 125Hz, ($\frac{1,024}{125}$) $\approx$ 8.192 seconds long. We experimented by using one part as a test set and the other three parts as a train set, as NABNet [9] did. The training set and test set comprise 9,000 and 3,000 records, respectively. The data from the same patient is not included in the training and test sets, simultaneously, so each fold ensures objectivity and generalizability.

4.2 Metric

For evaluation, we used metrics (or standards) proposed by two organizations: **the British Hypertension Society (BHS)** and **the Association for the Advancement of Medical Instrumentation (AAMI)**. The BHS and AAMI standards are designed to evaluate BP measurement methods and devices.

The BHS standard is based on the absolute difference between predicted and actual values. As shown in Table 1, according to the BHS standards, the grades are divided into four categories based on the percentage of absolute difference less than or equal to 5mmHg, 10mmHg, and 15mmHg for the predicted results. To get Grade A, for example, all percentages of the absolute difference less than or equal to 5, 10, and 15 mmHg in experiments should be more than 60%, 85%, and 95%, respectively. Also, we used the Mean Absolute Error (MAE) as an evaluation metric to show the performance statistically. MAE is defined as

$$MAE = \frac{\sum_{i=1}^{n} \left| Y_i - \hat{Y}_i \right|}{n}, \tag{2}$$

where $\hat{Y} = \left\{ \hat{Y}_1, \hat{Y}_2, \cdots, \hat{Y}_n \right\}$ and $Y = \left\{ Y_1, Y_2, \cdots, Y_n \right\}$ signify the predicted ABP waveform and the ground truth waveform, respectively.

According to the AAMI standard, the number of subjects participating in the evaluation should be more than or equal to 85. As shown in Table 2, the absolute values of the Mean Error (ME) and Standard Deviation (SD) should be less than or equal to 5 mmHg and 8 mmHg, respectively.

4.3 Implementation Details

We experiment with a machine equipped with an NVIDIA GeForce RTX 4090 GPU using the Pytorch library. We use the same preprocessing steps as NABNet [9] and ShallowNet [10]. The PPG and ECG signals of all records are normalized using the z-score method, and these signals are scaled to a range of 0 to 1. Also, the target ABP waveform is normalized using the z-score method. The SBP and DBP values across all records range from 75 to 190 and 50 to 120, respectively. The BP segments having differences between SBP and DBP values less than 20 and more than 120 were removed. In the DoG attention block, two Gaussian Filters were used with SD set to 7 Hz and 10 Hz, respectively.

4.4 Results

Quantitative Results We evaluate the performance of our model using key metrics defined by the BHS and the AAMI, presenting the results to demonstrate the effectiveness and performance of our approach.

BHS Standard Results: Under the BHS criteria, our performance was evaluated using several metrics, including MAE. This multifaceted assessment demonstrates the robustness and reliability of our research in estimating SBP, DBP, and MAP, among other key indicators. The evaluation revealed that the proposed method achieved an MAE of 2.22 mmHg for SBP, illustrating its capability to accurately measure systolic pressures, which are crucial for diagnosing and managing hypertension. In Table 3, the proposed method demonstrated an MAE of 1.92 mmHg for MAP, providing a consistent indicator of cardiovascular health and illustrating its effectiveness in capturing accurate arterial pressures across various physiological states. Additionally, the proposed method demonstrated a reasonable performance in estimating DBP with an MAE of 1.16 mmHg, and it is reliable in assessing the minimum arterial pressure during the heart relaxation phase. In Tables 4 to 6, the proposed method demonstrates exceptionally high performance in estimating SBP and MAP, surpassing the results of other recent studies. These findings provide a robust validation of the proposed method in BP monitoring. In Table 4, the proposed method achieved remarkable performance in SBP estimations with a 92.47% accuracy at the 5 mmHg threshold, increasing to 99.40% at the 10 mmHg threshold and reaching an impressive 99.88% at the 15 mmHg threshold. This performance is notably superior compared to other methods reported in the same table, where the closest competitor achieved a maximum of 88.72% accuracy at the 5 mmHg threshold. Similarly, in MAP estimations shown in Table 5, the proposed method demonstrated superior performance with 93.86% accuracy at the 5 mmHg threshold, 99.65% at the 10 mmHg, and 99.98% at the 15 mmHg threshold-significantly higher compared to other studies, with the closest competitor achieving 90.15% at the 5 mmHg threshold. In Table 6, our results for DBP estimation also showed better performance, with accuracies of 99.50% at the 5 mmHg, 99.98% at the 10 mmHg, and 100.00% at the 15 mmHg thresholds. These results demonstrate the overall efficacy of the proposed method across all primary indicators of BP.

AAMI Standard Results: In Table 7, we evaluate the performance metrics of DBP, MAP, and SBP with the existing methods, facilitating a direct evaluation of the proposed

Table 3: MAE in blood pressure estimation DBP, MAP, and SBP for the various method and the proposed method according to the BHS standards.

Method	Dataset	Input Signal	BHS-MAE		
			DBP	MAP	SBP
ABP-Net [3]	MIMIC-II	PPG, VPG, APG	3.73	3.30	6.41
Tasbiraha [1]	MIMIC-III	PPG	1.97	2.17	3.68
RDAE [12]	MIMIC-II	PPG	4.11	3.83	7.95
PPG2ABP [6]	MIMIC-III	PPG	3.45	2.31	5.73
Hybrid [15]	MIMIC-I	PPG	2.10	*2.10*	3.00
NABNet [9]	MIMIC-III	PPG, VPG, APG, ECG	**1.09**	2.37	*2.63*
SE-MSResUNet [8]	MIMIC-II	PPG	2.16	2.29	3.88
Ours	MIMIC-III	PPG	*1.16*	**1.92**	**2.22**

Table 4: The accuracy of the various methods and the proposed method against the BHS standard at 5mmHg, 10mmHg, and 15mmHg error margins in SBP estimation.

Method	Dataset	Input Signal	SBP		
			5mmHg	10mmHg	15mmHg
ABP-Net [3]	MIMIC-II	PPG, VPG, APG	51.71	78.72	90.19
RDAE [12]	MIMIC-II	PPG	46.30	72.10	85.20
BP-Net [14]	MIMIC-II	PPG	69.21	86.01	92.19
PPG2ABP [6]	MIMIC-III	PPG	70.81	85.30	90.92
NABNet [9]	MIMIC-III	PPG, VPG, APG, ECG	*88.72*	*99.02*	*99.84*
SE-MSResUNet [8]	MIMIC-II	PPG	76.54	92.56	96.72
Ours	MIMIC-III	PPG	**92.47**	**99.40**	**99.88**

Table 5: The accuracy of the various methods and the proposed method against the BHS standard at 5mmHg, 10mmHg, and 15mmHg error margins in MAP estimation.

Method	Dataset	Input Signal	MAP		
			5mmHg	10mmHg	15mmHg
ABP-Net [3]	MIMIC-II	PPG, VPG, APG	77.39	93.35	98.36
RDAE [12]	MIMIC-II	PPG	76.00	92.30	96.90
BP-Net [14]	MIMIC-II	PPG	85.64	94.40	97.68
PPG2ABP [6]	MIMIC-III	PPG	87.38	95.17	97.73
NABNet [9]	MIMIC-III	PPG, VPG, APG, ECG	87.58	**99.82**	**99.99**
SE-MSResUNet [8]	MIMIC-II	PPG	*90.15*	97.84	99.27
Ours	MIMIC-III	PPG	**93.86**	*99.65*	*99.98*

method against the existing methods. For the metrics of DBP, MAP, and SBP, Ours shows reasonable performances. Although the performances of the proposed method are not the best for DBP and SBP, that for MAP shows the second-best performance. The proposed method achieved a ME of -0.373 mmHg and a SD of 1.467 mmHg for DBP. For SBP, the proposed method demonstrated a reliable measurement with an ME of 0.999 mmHg and an SD of 2.770 mmHg. Different from DBP and SBP, although

Table 6: The accuracy of the various methods and the proposed method against the BHS standard at 5mmHg, 10mmHg, and 15mmHg error margins in DBP estimation.

Method	Dataset	Input Signal	DBP		
			5mmHg	10mmHg	15mmHg
ABP-Net [3]	MIMIC-II	PPG, VPG, APG	70.25	93.35	98.36
RDAE [12]	MIMIC-II	PPG	73.20	91.90	97.00
BP-Net [14]	MIMIC-II	PPG	84.34	95.19	98.14
PPG2ABP [6]	MIMIC-III	PPG	82.84	92.16	95.73
NABNet [9]	MIMIC-III	PPG, VPG, APG, ECG	**99.59**	**99.99**	**100.00**
SE-MSResUNet [8]	MIMIC-II	PPG	91.65	98.24	*99.35*
Ours	MIMIC-III	PPG	*99.50*	*99.98*	**100.00**

Table 7: The AAMI standard results show the ME and SD for DBP, MAP, and SBP estimations across the various methods and the proposed method.

Method	Dataset	AAMI					
		DBP		MAP		SBP	
		ME	SD	ME	SD	ME	SE
ABP-Net [3]	MIMIC-II	*-0.280*	5.810	-0.940	5.320	1.640	7.420
RDAE [12]	MIMIC-II	-0.417	5.504	**0.204**	5.130	1.447	10.372
BP-Net [14]	MIMIC-II	0.594	4.778	0.425	4.784	**-0.225**	8.504
PPG2ABP [6]	MIMIC-III	1.619	6.859	0.631	4.962	-1.582	10.688
NABNet [9]	MIMIC-III	-0.342	**1.059**	-0.678	*2.969*	-0.678	*2.969*
SE-MSResUNet [8]	MIMIC-II	**-0.110**	3.750	*-0.210*	3.720	*-0.440*	6.170
Ours	MIMIC-III	-0.373	*1.467*	0.296	**2.580**	0.999	**2.770**

our MAP results were not the best-performing, they were the second-best with a ME of 0.296 mmHg and a SD of 2.580 mmHg. These results demonstrate that the proposed method provides reasonable and clinically valuable performance,

Qualitative Results Fig. 4 shows the reconstructed ABP waveform from the input PPG signals. In each sub-figure, the first to third rows represent the raw PPG signal, the normalized ABP waveform, and the denormalized ABP waveform. While Fig. 4b and Fig. 4c represent stable scenarios with consistent and regular PPG signal, Fig. 4a illustrates a scenario with notable signal instability, red-boxed by irregular fluctuations in amplitude and rhythm. MAE is a critical metric in this analysis. In the unstable PPG input shown in Fig. 4a, the MAE spikes to 6.106, much higher than the MAEs of 2.402 and 2.786 observed in the more stable inputs. This marked difference in MAE values clearly shows how much signal instability can degrade the quality of health monitoring outputs, emphasizing the need for high-quality, stable input signals to achieve accurate health assessments. This comparison not only highlights the challenges posed by signal variability but also points to the potential for technological enhancements to improve the reliability of non-invasive health monitoring systems.

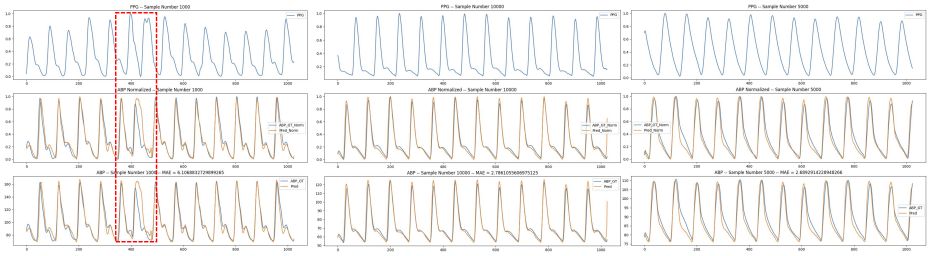

(a) Unstable PPG input (b) Stable PPG input1 (c) Stable PPG input2

Fig. 4: Comparison of reconstructed ABP waveforms from PPG signals, demonstrating the impact of signal stability. (a) Displays waveforms from an unstable PPG input, while (b) and (c) show waveforms from stable PPG inputs.

5 Conclusion

In this paper, the proposed method demonstrated the feasibility and reliability of using solely PPG signal for ABP waveform reconstruction. The breakthrough of the proposed method has substantial potential to influence the wearable device market and the broader healthcare industry. A single PPG signal without an ECG signal not only simplifies the technological requirements but also enhances accessibility and usability. Incorporation of our model into wearable or sensing technologies could transform how continuous monitoring is approached, particularly for patients with cardiovascular conditions. Wearable devices equipped with our PPG-based method could offer real-time insights into a user's cardiovascular health, alerting users and healthcare providers to potential health issues before they become severe. This proactive approach to health management not only promises to improve individual outcomes but also has the potential to reduce the overall burden on healthcare systems. This progress is expected to enhance user adoption, increase patient engagement in their health monitoring, and ultimately improve the healthcare ecosystem.

Acknowledgment This work was supported by Artificial intelligence industrial convergence cluster development project funded by the Ministry of Science and ICT(MSIT, Korea)Gwangju Metropolitan City.

References

1. Athaya, T., Choi, S.: An estimation method of continuous non-invasive arterial blood pressure waveform using photoplethysmography: A u-net architecture-based approach. Sensors 21(5) (2021)
2. BN, S., Srinivasa, R.S., Malur Saidutta, Y., Cho, J., Lee, C.H., Yang, C., Shen, Y., Jin, H.: End-to-end personalized cuff-less blood pressure monitoring using ecg and ppg signals. In: ICASSP 2024 - 2024 IEEE International Conference on Acoustics, Speech and Signal Processing (ICASSP). pp. 2101–2105 (2024)
3. Cheng, J., Xu, Y., Song, R., Liu, Y., Li, C., Chen, X.: Prediction of arterial blood pressure waveforms from photoplethysmogram signals via fully convolutional neural networks. Computers in Biology and Medicine 138, 104877 (2021)

4. Fang, X., Shi, Y., Guo, Q., Wang, L., Liu, Z.: Sub-band based attention for robust polyp segmentation. In: Elkind, E. (ed.) Proceedings of the Thirty-Second International Joint Conference on Artificial Intelligence, IJCAI-23. pp. 736–744. International Joint Conferences on Artificial Intelligence Organization (8 2023), main Track
5. Fu, Y., Zeng, H., Ma, L., Ni, Z., Zhu, J., Ma, K.K.: Screen content image quality assessment using multi-scale difference of gaussian. IEEE Transactions on Circuits and Systems for Video Technology 28(9), 2428–2432 (2018)
6. Ibtehaz, N., Mahmud, S., Chowdhury, M.E., Khandakar, A., Salman Khan, M., Ayari, M.A., Tahir, A.M., Rahman, M.S.: Ppg2abp: Translating photoplethysmogram (ppg) signals to arterial blood pressure (abp) waveforms. Bioengineering 9(11), 692 (2022)
7. Kim, T.H., Bao, C., Chen, Z., Kim, W.S.: 3d printed leech-inspired origami dry electrodes for electrophysiology sensing robots. npj Flexible Electronics 6 (12 2022)
8. Ma, K., Zou, L., Yang, F., Zhan, C.A., Gong, Y., Huang, D.: Continuous non-invasive arterial blood pressure monitoring with photoplethysmography via se-msresunet network. Biomedical Signal Processing and Control 90, 105862 (2024)
9. Mahmud, S., Ibtehaz, N., Khandakar, A., Sohel Rahman, M., JR. Gonzales, A., Rahman, T., Shafayet Hossain, M., Sakib Abrar Hossain, M., Ahasan Atick Faisal, M., Fuad Abir, F., Musharavati, F., E. H. Chowdhury, M.: Nabnet: A nested attention-guided biconvlstm network for a robust prediction of blood pressure components from reconstructed arterial blood pressure waveforms using ppg and ecg signals. Biomedical Signal Processing and Control 79, 104247 (2023)
10. Mahmud, S., Ibtehaz, N., Khandakar, A., Tahir, A.M., Rahman, T., Islam, K.R., Hossain, M.S., Rahman, M.S., Musharavati, F., Ayari, M.A., Islam, M.T., Chowdhury, M.E.H.: A shallow u-net architecture for reliably predicting blood pressure (bp) from photoplethysmogram (ppg) and electrocardiogram (ecg) signals. Sensors 22(3) (2022)
11. Pickering, T.G., Hall, J.E., Appel, L.J., Falkner, B.E., Graves, J., Hill, M.N., Jones, D.W., Kurtz, T., Sheps, S.G., Roccella, E.J.: Recommendations for blood pressure measurement in humans and experimental animals. Circulation 111(5), 697–716 (2005)
12. Qin, K., Huang, W., Zhang, T.: Deep generative model with domain adversarial training for predicting arterial blood pressure waveform from photoplethysmogram signal. Biomedical Signal Processing and Control 70, 102972 (2021)
13. Rapsomaniki, E., Timmis, A., George, J., Pujades-Rodriguez, M., Shah, A.D., Denaxas, S., White, I.R., Caulfield, M.J., Deanfield, J.E., Smeeth, L., et al.: Blood pressure and incidence of twelve cardiovascular diseases: lifetime risks, healthy life-years lost, and age-specific associations in 1· 25 million people. The Lancet 383(9932), 1899–1911 (2014)
14. Rishi Vardhan, K., Vedanth, S., Poojah, G., Abhishek, K., Nitish Kumar, M., Vijayaraghavan, V.: Bp-net: Efficient deep learning for continuous arterial blood pressure estimation using photoplethysmogram. In: 2021 20th IEEE International Conference on Machine Learning and Applications (ICMLA). pp. 1495–1500 (2021)
15. Shi, W., Zhou, C., Zhang, Y., Li, K., Ren, X., Liu, H., Ye, X.: Hybrid modeling on reconstitution of continuous arterial blood pressure using finger photoplethysmography. Biomedical Signal Processing and Control 85, 104972 (2023)
16. Yang, H., Li, C., Liang, Y., Liu, W., Meng, F.: Calibrated convolution with gaussian of difference. Applied Sciences 12(13) (2022)
17. Yazdi, R., Khotanlou, H., Alighardash, E., Zolfaghari, M.: Edge detection method based on the differences in intensities of rotating kernel borders. In: 2023 6th International Conference on Pattern Recognition and Image Analysis (IPRIA). pp. 1–5 (2023)
18. Zhang, J., Zhao, Z.: Optimized gaussian filter motion image background processing. In: 2022 IEEE International Conference on Advances in Electrical Engineering and Computer Applications (AEECA). pp. 633–636 (2022)